Label-free DNA detection platform based on atomic force microscopy visualisation : Characterising the molecular-recognition-triggered conformational changes of an immobilised receptor oligonucleotide probe

Nakano, Koji
Department of Applied Chemistry, Faculty of Engineering, Kyushu University

Yamanouchi, Hirokazu
Department of Applied Chemistry, Faculty of Engineering, Kyushu University

Yoshinaga, Hisao
Department of Applied Chemistry, Faculty of Engineering, Kyushu University

Soh, Nobuaki
Department of Applied Chemistry, Faculty of Engineering, Kyushu University

他

出版情報：Chemical Communications. 46 (31), pp.5683-5685, 2010-08-21. Royal Society of Chemistry
バージョン：

Label-free DNA detection platform based on atomic force microscopy visualisation: characterising the molecular-recognition-triggered conformational changes of an immobilised receptor oligonucleotide probe

Koji Nakano,* Hirokazu Yamanouchi, Hisao Yoshinaga, Nobuaki Soh, and Toshihiko Imato

Using atomic microscopy imaging, probe DNA sequence self-assemblies developed on Si(100) substrates undergo a conformational transition from an extended stem-loop structure to a double helix; such assemblies readily report on DNA molecular recognition events and should be suitable as a label-free, DNA hybridisation assay platform.

The last decade has seen a wealth of research about electrode-attached DNA probes for a large body of applications ranging from simple biosensors to modern high-throughput analysis devices.[1] In recent years, such probes have become increasingly sophisticated: particularly those regarding conformational changes of synthetic oligodeoxynucleotides (ODN) have formed the basis of target DNA detection. Anne and co-workers reported a model system consisting of an electrode-attached ODN probe labelled at its 3'-end with ferrocene, which can produce electrochemical responses upon a conformation change to a double helix structure.[2a] This strategy has been extended to a molecular hairpin-like DNA[2b,c] or a peptide-nucleic acid.[3] Furthermore, the adaptation of aptamers has led to a dramatic increase in research activities in this field.[4]

Currently, electrochemistry has been primarily used to characterise these kinds of ODN adlayers, including the quantification of target DNA responses. Nanotechnology methods have rarely detected or analysed ODN adlayers. Grinstaff's group has reported the only example, *i.e.*, film-thickness analysis using atomic force microscopy (AFM).[2c] This type of height measurement have been used to detect label-free DNA hybridisation based on changes of smoothness,[5a] height,[5b] density,[5c] and further have been investigated for single-base mismatch detection using locked nucleic acid-integrated hairpin DNA probes.[5d] In this paper, we present a direct visualisation of the surface adlayer at a single-ODN-level. A molecular hairpin-like DNA was self-assembled on to Si(100) substrates whose surface was modified with thiol-presenting alkoxysilane monolayers beforehand (Scheme 1). Taking advantage of a DNA stem-loop to double-helix conformational transition facilitated a non-label and straightforward method for detecting hybridisation.

Molecular observation of DNA self-assembly inevitably requires a substrate to present an atomically flat surface over a considerably large region, typically 100 × 100 square nanometres as a minimum. Consequently, silicon wafers with (100) texture were selected. Following the two-step pretreatment, the substrate was subjected to chemical vapour adsorption (CVA)[6] using 3-mercaptopropyl-trimethoxysilane (MPTS) to render the surface reactive. Subsequently, the probe ODN molecules (**p28**[2b]), which were annealed at the intracatenary sequences (the underlined bases) beforehand to form a single-stranded loop, self-assembled onto the MPTS/Si substrate surface. The base sequence is shown below together with that of the target (**t27**) and the control (**c27**) DNA sequences.

p28 5'GCGAGGTAAAACGACGGCCAGTCCTCGCC$_3$H$_6$SH3'
t27 5'TTTTTACTGGCCGTCGTTTTACTCTTT3'
c27 5'TTTTTGTCAATTACTACCCCGTTCTTT3'

Examination of the substrate by x-ray photoelectron spectroscopy (XPS) analysis confirmed that the surface phase formed reflects the adsorbates intended. Initially, wide-scan XPS spectra for the MPTS/Si and the **p28**/MPTS/Si substrates were recorded and revealed the principle peaks for Si 2p, P 2p, S 2p, C 1s, N 1s and O 1s; elements that constitute the surface phase.[7a,b] We also acquired the XPS spectra for each constituent element. Among the spectra recorded, a line-shape analysis on the C 1s core region signal suggested that the main peak at 283 eV was associated with some weaker features at 285 and 287 eV. These weaker features are ascribed to the particular chemical shift for C–O (C–N) and

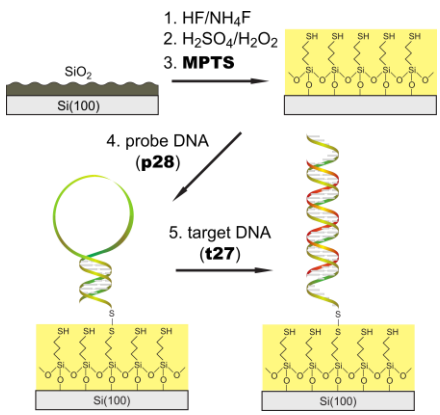

Fig. 1 Schematic illustration of the formation of the intended surface-phase.

C=O (C=N) functions in **p28**. The N 1s signal, on the other hand, was possibly ascribed to the photoelectrons for the intracyclic N and exocyclic NH_2 functions. This kind of DNA-immobilisation is known to occur via the formation of a disulfide bond between the thiol group in the MPTS monolayer and the 3'-thiol in the DNA oligo.[7c] The XPS didnot distinguish between the disulfide and the thiol in the surface adlayer. However, we found that by comparing with alkanethiol monolayer data,[7d] the binding energy was closer to that for the unbound thiol rather than that for the alkanethiolate–Au complex.

Definite mass increments are associated with the MPTS and the **p28** modifications as determined by gravimetric analysis using a quartz-crystal microbalance (QCM). For MPTS self-assembled monolayers (SAMs), we observed a specific resonant frequency decrease of 89 ± 18 Hz (n = 4), which is equivalent to 1.5 ± 0.30 nmol cm^{-2} of surface coverage when the Sauerbrey's equation[8] is adopted. Although a clean Si(100) exhibits a mixed-lattice structure that predicts a rather complicated adlayer structure, we simply assumed a hypothetical surface species, $HS\text{-}C_3H_6\text{-}Si\text{-}(OCH_3)_3$. A semi-empirical MO calculation determined the surface occupied area, which is equivalent to an equilateral triangle with a slide of 0.36 nm, i.e. the apparent distance between the sp3 carbon atoms in the anchor $\text{-}Si(OCH_3)_3$. This gives rise to a 3.0 nmol cm^{-2} surface concentration at saturation, which suggests that MPTS adsorbs to form submonolayers. Additionally, the QCM experiments have characterised the probe DNA immobilisation including hybridisation: we obtained particular surface concentrations of 53 pmol cm^{-2} for **p28** and 31 pmol cm^{-2} for the hybridisation binding of **t27**. Cory-Pauling-Koltun model building indicate the cross-section for the **p28** single-stranded loop is 5.0 nm^2 (1.2 × 4.2 nm). This is equivalent to a theoretical coverage of 33 pmol cm^{-2}. Thus, the experimental data obtained seems reasonable. The hybridisation efficiency was 58% and in general agreement with literature data.[9]

Exploring AFM experiments using the intermitted contact mode imaging confirmed that the substrates afford a permissible flatness within ±0.05 nm over a few μm regions following the cleanup. In contrast, this type of imaging only gave surface topographic images with single-ODN-molecules unresolved. This was improved by noncontact-mode imaging (Fig. 2). With the CVA-treated substrate, there were clear irregular, yet delicate, features observed (6 nm in diameter as measured in the AFM image). We have attributed each of the surface entities to single MPTS molecules since the mercaptopropyl tail gives a 1.3 nm-diameter trace by rotation. The attachment of the **p28** oligo on the MTPS/Si substrate has been characterised by the presence of potentially ordered, observed somewhat irregularly though, surface physical matters; they are commonly found as spheroid hemispheres (8 × 20 nm as observed in the AFM image). In contrast, hybridisation with **t27** produced surface topological images that are totally different; compact hemispheres (apparently 12 nm in diameter) are finely distributed covering the substrate surface almost completely. As a control, experiments using **c27** gave AFM images fundamentally similar to that of **p28** alone. The surface topological changes thus produced can be attributed to DNA hybridisation.

We have next examined the quantification of the surface morphology responses. Since the AFM images consist of a set of pixels, into which the particular height data are encoded, we will simply treat the height data based on histogram analysis. As seen in Fig. 3, plots showed that each frequency distribution fundamentally traces a specific curve, which is a typical normal distribution. Thus, the frequency profile was

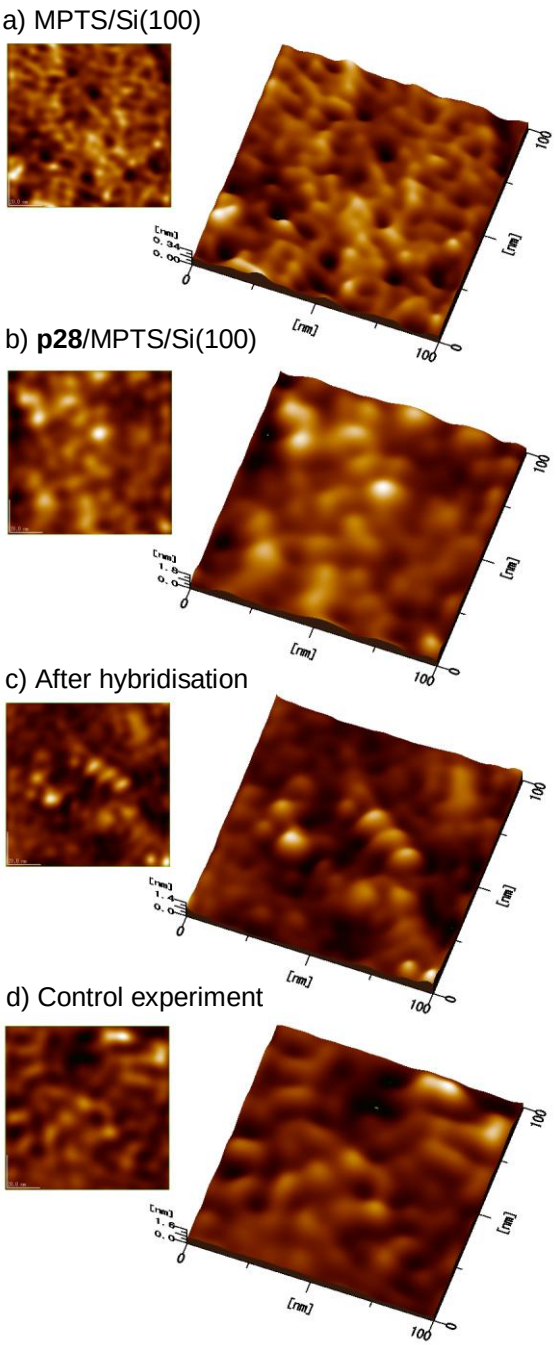

Fig. 2 Representative AFM images for the Si(100) substrates with the MPTS/Si (**a**), the **p28**/MPTS/Si interfacial structure (**b**) and changes of the surface topological structures by treating with **t27** (**c**) or **c27** (**d**). Each 2D image obtained is shown together with its 3D expression.

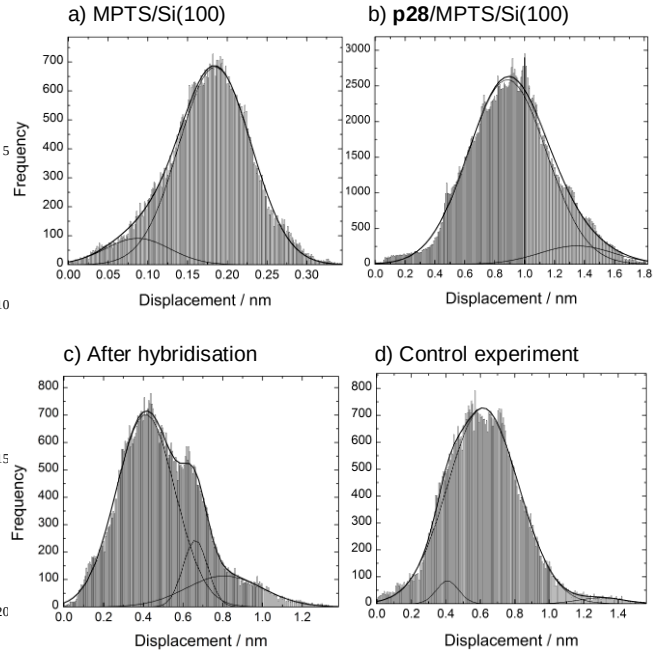

Fig. 3 Plots of the frequency distributions for the height data of each pixel in the corresponding AFM images. Panels represent the result for MPTS/Si (**a**), **p28**/MPTS/Si (**b**) and changes in the profile following treatment with **t27** (**c**) or **c27** (**d**). Plots were made for the entire AFM image which consisted of 256 × 256 pixels, except panel (**b**) which consisted of 512 × 512 pixels. Peak-fitting analysis assuming multiple Gauss-functions gave thin-line-peaks that successfully reproduce the experimental data as shown by the thick solid lines.

analysed by nonlinear curve fitting assuming a set of multiple peaks, in which, each peak is represented as a simple Gauss function.

As summarised in Table 1, the surface morphology response that has been visually recognized can be conveniently and quantitatively interpreted. For example, the MPTS/Si substrate shows a fine feature primarily at a displacement of 0.18 nm from the surface. This feature is presumably derived by the differences in the conformation at the mercaptomethyl terminus. A settle feature at 0.09 nm may reflect the irregularity of the Si substrate surface. Attachment of ODN onto the MPTS SAM increased the surface roughness, almost quintuple for the **p28** case: this can be reasonably ascribed to the spatial bulk for the single-stranded loop structure. Results were fairly reproducible to give a series of peak position data of 0.88, 1.0, and 1.1 nm for the three different experiments including sample preparations. Upon hybridisation, the molecular hairpin DNA probe transforms to the double helix structure that is defined by a cylindrical structure with a mechanical stiffness. Apparently the surface roughness reduced to one-half due to the more compact spatiality for the **p28**-**t27** double helix than that for the **p28** loop. Treatment with **t27** for hybridisation often gave extraordinary roughened surfaces, *ca*. 4 nm-height, probably due to inorganic precipitation from the buffer solution. However, a careful experiment improved reproducibility giving a pair of specific values of 0.47 and 0.63 nm even after hybridisation. In contrast, the surface remained roughly textured when the **p28**-substrate was treated with the control sample. It seems that the more detailed analysis for the peak-fitting data allows us to

Table 1 A summary of the peak-fitting analysis for the AFM image height data.

	Peak position and normalised peak area (%)						
	0.09 nm	0.18 nm	0.41 nm	0.49 nm	0.66 nm	0.88 nm	1.3 nm
MPTS/Si(100)	11	89					
p28/MPTS/Si(100)						91	9
After hybridisation			74	11	15		
Control experiment				3	95		2

access the analytical parameters involving the hybridisation efficiency, selectivity and limit of detection. We are currently characterising these points.

In conclusion, by taking advantage of the AFM visualisation read-out, we have developed a label-free, DNA molecular recognition platform using a hairpin-like DNA sequence as a reporter oligo. The delicate surface delayed reusability problem and left it as future task. But, we have achieved microscopic imaging of the conformational transition from an extended stem-loop structure to a double helix. These types of chemical sensing methods are useful in applications involving covalent label functions. The present system forms the basis of a sensing and diagnostic method that enables a complete label-free detection approach of target DNA molecules.

Acknowledgement. We thank Professor N. Kimizuka and Dr. K. Kuroiwa, Kyushu University for access to the XPS. K. N. acknowledges the financial support by the Precursory Research for Embryonic Science and Technology, the Japan Science and Technology Agency and by a Grant-in-Aid for Scientific Research from the Ministry of Education, Culture, Sports, Science and Technology (MEXT), Japan.

Notes and references

Department of Applied Chemistry, Faculty of Engineering, Kyushu University, 744 Motooka, Nishi-ku, Fukuoka 819-0395, Japan; E-mail: nakano@cstf.kyushu-u.ac.jp

† Electronic Supplementary Information (ESI) available: Experimental methods, additional AFM images, and XPS spectral data. See http://

1. E. Paleček, *Anal. Chem*., 2001, **73**, 75A–83A.
2. (a) A. Anne, A. Bouchardon, J. Moiroux, *J. Am. Chem. Soc*., 2003, **125**, 1112–1113. (b) C. Fan, K. W. Plaxco, Al. J. Heeger, *Proc. Nat. Acad. Sci. USA* 2003, **100**, 9134–9137. (c) C. E. Immoos, S. J. Lee, M. W. Grinstaff, *ChemBioChem*., 2004, **5**, 1100–1103.
3. H. Aoki, H. Tao, *Analyst (London),* 2007, **132**, 784–791.
4. (a) A.-E. Radi, J. L. A. Sanchez, E. Baldrich, C. K. O'Sullivan, *J. Am. Chem. Soc*., 2006, **128**, 117–124. (b) I. Willner, M. Zayats*, Angew. Chem. Int. Ed*., 2007, **46**, 6408–6418.
5. (a) M. Holmberg, A. Kühle, J. Garnæs, A. Boisen, *Ultramicroscopy*, 2003, **97**, 257-261. (b) D. Zhou, K. Sinniah, C. Abell, T. Rayment, *Angew. Chem. Int. Ed.*, 2003, **42**, 4934–4937. (c) M. Liu, G.-Y. Liu, *Langmuir*, 2005, **21**, 1972–1978. (d) W.-H. Han, J.-M. Liao, K.-L. Chen, S.-M. Wu, Y.-W. Chiang, S.-T. Lo, C.-L. Chen, C.-M. Chiang, *Anal. Chem*., 2010, **82**, 2395–2400.
6. T. Koga, M. Morita, H. Ishida, H. Yakabe, S. Sasaki, O. Sakata, H. Otsuka, A. Takahara, *Langmuir,* 2005, **21**, 905–910.
7. (a) B. A. Cavic, M. E. McGovern, R. Nisman, M. Thompson, *Analyst* 2001, **126**, 485–490. (b) D. Y. Petrovykh, H. Kimura-Suda, L. J. Whitman, M. J. Tarlov, *J. Am. Chem. Soc*., 2003, **125**, 5219–5226. (c) R. Lenigk, M. Carles, N. Y. Ip, J. S. Sucher, *Langmuir,* 2001, **17**, 2497–2501. (d) D. G. Castner, K. Hinds, D. W. Grainger, *Langmuir,* 1996, **12**, 5083–5086.
8. G. Z. Sauerbrey, *Z. Phys.*, 1959, **155**, 206–222.
9. A. Peterson, R. J. Heaton, R. M. Georgiadis, *Nucleic Acids Res*., 2001, **29**, 5163–5168.